

## EXPANSION OF KES 73, A SHELL SUPERNOVA REMNANT CONTAINING A MAGNETAR

KAZIMIERZ J. BORKOWSKI<sup>1</sup> AND STEPHEN P. REYNOLDS<sup>1</sup>

<sup>1</sup>*Department of Physics, North Carolina State University, Raleigh, NC 27695-8202, USA*

(Received May 16, 2017; Accepted July 28, 2017)

### ABSTRACT

Of the 30 or so Galactic magnetars, about 8 are in supernova remnants (SNRs). One of the most extreme magnetars, 1E 1841-045, is at the center of the SNR Kes 73 (G27.4+0.0), whose age is uncertain. We measure its expansion using three *Chandra* observations over 15 yr, obtaining a mean rate of  $0.023\% \pm 0.002\% \text{ yr}^{-1}$ . For a distance of 8.5 kpc, we obtain a shell velocity of  $1100 \text{ km s}^{-1}$  and infer a blast-wave speed of  $1400 \text{ km s}^{-1}$ . For Sedov expansion into a uniform medium, this gives an age of 1800 yr. Derived emission measures imply an ambient density of about  $2 \text{ cm}^{-3}$  and an upper limit on the swept-up mass of about  $70 M_{\odot}$ , with lower limits of tens of  $M_{\odot}$ , confirming that Kes 73 is in an advanced evolutionary stage. Our spectral analysis shows no evidence for enhanced abundances as would be expected from a massive progenitor. Our derived total energy is  $1.9 \times 10^{51} \text{ erg}$ , giving a very conservative lower limit to the magnetar's initial period of about 3 ms, unless its energy was lost by non-electromagnetic means. We see no evidence of a wind-blown bubble as would be produced by a massive progenitor, or any evidence that the progenitor of Kes 73/1E 1841-045 was anything but a normal red supergiant producing a Type IIP supernova, though a short-lived stripped-envelope progenitor cannot be absolutely excluded. Kes 73's magnetar thus joins SGR 1900+14 as magnetars resulting from relatively low-mass progenitors.

*Keywords:* ISM: individual objects (Kes 73) — ISM: supernova remnants — X-rays: ISM

arXiv:1708.01626v1 [astro-ph.HE] 4 Aug 2017

## 1. INTRODUCTION

Magnetars, young neutron stars with surface magnetic fields  $B \gtrsim 5 \times 10^{13}$  G, are expected to be born with rotation periods of order milliseconds and hence with rotational energies comparable to the energy released in a supernova (see [Kaspi & Beloborodov 2017](#), hereafter KB17, for a recent review). Their current rotation periods of 2 – 12 s are consistent with standard dipole spindown as for typical rotation-powered pulsars with lower magnetic fields. Much is uncertain about magnetars, including their progenitors, birth properties, magnetic-field and thermal evolution, and effects on the explosions that produce them. Even the ages of the 30 or so Galactic magnetars are not well constrained; spindown ages ( $P/2\dot{P}$ ) are known for about 20, but may not reflect true ages. If the magnetic fields result from dynamo action in the neutron-star core, periods of no more than a few ms are required ([Duncan & Thompson 1992](#); [Spruit 2009](#)). Fossil fields have also been proposed as the origin of the high magnetic fields, e.g., [Ferrario & Wickramasinghe \(2006\)](#), but such models have significant problems accounting for some properties of magnetars ([Spruit 2008](#)). Rotation at a few ms periods would be difficult to understand if the proto-neutron star magnetic field is coupled to an extended envelope, so for this and other reasons (including the small scale height, 20 – 30 pc, of their Galactic distribution; [Olausen & Kaspi 2014](#)), magnetars are often assumed to come from massive progenitors that explode as stripped-core supernovae after heavy mass loss, perhaps distinguishing them from normal pulsars whose birth periods are thought to be considerably longer (ca. 100 ms; see, e.g., [Gullón et al. 2015](#)).

Several magnetars inhabit supernova remnants (8 – 10; KB17), and analysis of the remnants has been brought to bear to constrain the properties of their magnetars. [Vink & Kuiper \(2006\)](#) showed that for three SNR/magnetar pairs, the deduced explosion energies were typical for supernovae, constraining initial magnetar rotation periods to  $P_0 \gtrsim 5$  ms (unless somehow the magnetar energy lost is not imparted to the ejecta, for instance as neutrinos or gravitational radiation). [Martin et al. \(2014\)](#) showed that the same three SNRs do not differ in X-ray luminosity or spectrum (abundances and ionization state) from remnants hosting normal pulsars.

Since the spindown age is not a reliable indicator of true age for magnetars (KB17), a more direct measure is the observation of expansion proper motions, possible with *Chandra* for the expected shock velocities of order  $1000 \text{ km s}^{-1}$  or greater. Here we report observations of the expansion of the X-ray remnant Kes 73 (G27.4+0.0) which constrain its age.

As documented in KB17, the magnetar in Kes 73, 1E 1841-045, has a period of 11.8 s (the longest of 30 or so), an X-ray quiescent luminosity of  $1.8 \times 10^{35} \text{ erg s}^{-1}$  between 2 and 10 keV, for a distance of 8.5 kpc ([Tian & Leahy 2008](#)) (second highest, after SGR 0526–66 in the LMC), and a spin-inferred magnetic field of  $7.0 \times 10^{14}$  G, behind only that for SGR 1900+14 and the recently increased value for SGR 1806-20 ( $2 \times 10^{15}$  G; [Younes et al. 2015](#)). Its spindown age of 4600 yr is not atypical. It has exhibited typical magnetar bursting

Table 1. *Chandra* Imaging Observations of Kes 73.

Date	Observation ID	Roll Angle (deg)	Effective Exposure Time (ks)
2000 Jul 23–24	729	235	29.26
2006 Jun 30	6732	242	24.86
2015 Jun 04–05	16950	129	28.65
2015 Jul 07	17668	201	20.88
2015 Jul 08–09	17692	201	23.26
2015 Jul 09–10	17693	201	22.57

behavior. An extended *Fermi* source includes the location of Kes 73 ([Li et al. 2017](#); [Yeung et al. 2017](#)), but it is four times larger and we consider the association improbable.

Kes 73 was among the systems examined by [Vink & Kuiper \(2006\)](#). A detailed X-ray study was performed by [Kumar et al. \(2014\)](#), who report an age between 750 and 2100 yr and an explosion energy of about  $3 \times 10^{50}$  erg, based on two-component plane-shock spectral fits. They also report enhanced abundances of Si and S for one component, which they attribute to ejecta.

## 2. OBSERVATIONS

*Chandra* observed Kes 73 in 2000 (Epoch I) and 2006 (Epoch II). Our Epoch III observations took place in 2015 June and July in 4 individual pointings (Table 1), with the remnant again placed on the Advanced CCD Imaging Spectrometer (ACIS) S3 chip. Observations were reprocessed with CIAO version 4.8 and CALDB version 4.7.1, then screened for periods of high particle background. Very Faint mode was used; the total effective exposure time is 95.4 ks.

We aligned the first three 2015 pointings to the reference frame of the 2015 Jul 09–10 observation (Obs. 17693) using photons from the remnant itself, a variation of our more general method for measuring expansion, described below. Only an image extracted from the longest (28.7 ks) pointing from 2015 June (Obs. 16950) required smoothing; shifts between this and other pointings were found using unsmoothed images.

The XSPEC spectral analysis package ([Arnaud 1996](#)) was used to study X-ray spectra extracted from individual observations and added together to obtain merged spectra (response files were averaged). In our spectral fits, we relied on nonequilibrium ionization (NEI) models based on APEC NEI version 2.0 atomic data ([Smith et al. 2001](#)), augmented with inner-shell atomic data as described in [Badenes et al. \(2006\)](#) and [Borkowski et al. \(2013\)](#).

Archival *Chandra* imaging observations of Kes 73 from 2000 July and 2006 June (Table 1) were reprocessed in the same way as the Epoch III observations. The Faint mode was

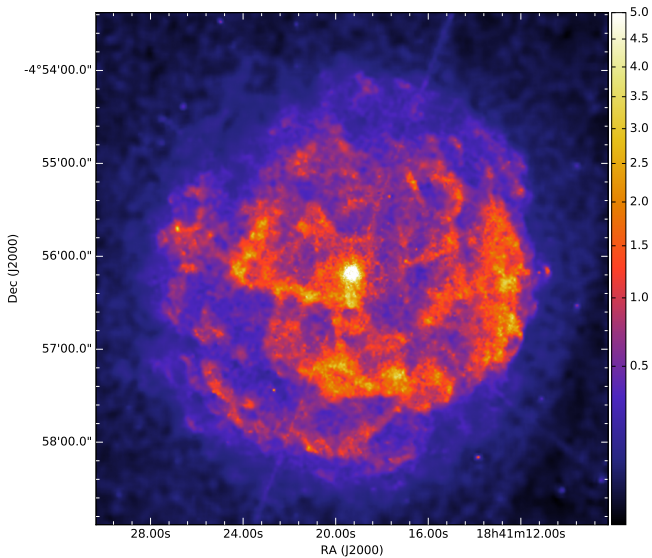


**Figure 1.** Smoothed X-ray image of Kes 73 in the 0.8–8 keV energy range from 2015. The bright magnetar at its center is saturated. The scale is in counts per  $0''.323 \times 0''.323$  image pixel.

employed in these Epoch I and II observations instead of the Very Faint mode, so their particle background is higher than at Epoch III. As discussed next, their alignment to the 2015 Jul 09–10 observation was done while measuring expansion.

### 3. EXPANSION

The time baseline between the 29 ks 2000 and 95 ks 2015 *Chandra* observations is almost 15 yr. In order to measure expansion, we use the method of [Carlton et al. \(2011\)](#) and [Borkowski et al. \(2016\)](#). First, we extracted a data cube from the merged 2015 observations,  $1024^2 \times 64$  in size, and in the energy range from 0.8 to 8 keV. The spatial pixel size is  $0''.323 \times 0''.323$  (slightly less than  $2/3$  of ACIS  $0''.492$  pixel). We then smoothed this data cube with the multiscale partitioning method of [Krishnamurthy et al. \(2010\)](#). We set the penalty parameter that controls smoothing to 0.015, the value that we found optimal for G11.2–0.3 ([Borkowski et al. 2016](#)).

A smoothed image is shown in Figure 1. We used this image as a model for measuring expansion (after subtraction of background, assumed to be uniform across the remnant, and normalization by the monochromatic ( $E = 1.49$  keV) exposure map). The maximum-likelihood method of [Cash \(1979\)](#) was employed to fit the smoothed 2015 image to the earlier raw images strongly affected by Poisson noise. In addition to varying the image scale in these fits, we also allowed for changes in the overall surface brightness by fitting for the surface brightness scale factor  $S$ . We also allowed for variations in image shifts in R.A. and declination, so the image alignment was done simultaneously with expansion measurements. We accounted for spatial variations in the effective

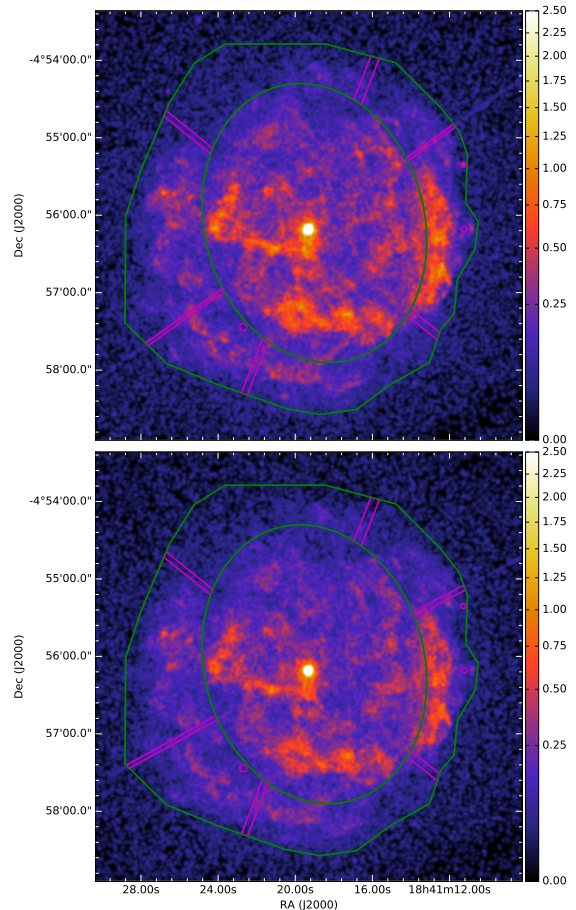


**Figure 2.** X-ray images of Kes 73 in the 0.8–8 keV energy range from 2000 (top) and 2006 (bottom), smoothed with a Gaussian kernel with  $\text{FWHM} = 2''.3$ . The outer shell chosen for expansion measurements is demarcated by an ellipse and a polygon (in green), with regions affected by out-of-time events and point sources masked out (in magenta). The scales are in counts per image pixel.

exposure time at Epochs I and II with monochromatic exposure maps, and for the higher background rate at these epochs relative to Epoch III.

The spatial morphology of Kes 73 is complex, consisting of overlapping inner and outer shells, and with bright and clumpy X-ray emission seen elsewhere within the remnant’s interior (Fig. 1). The outer shell most likely traces the location of the blast wave, while the origin of the interior emission is not clear. Our expansion measurements are restricted to the outer shell (see masks shown in Figures 2) where proper motions are expected to be largest. We assume uniform expansion there, an assumption that is expected to hold even in the presence of a large density gradient in the ambient medium ([Williams et al. 2013](#)). Point sources were excluded. We also excluded regions affected by “out-of-time” events caused by photons from the bright, piled-up magnetar that were detected during the ACIS S3 chip readout, producing the radial “streaks” centered on the magnetar in Figures 1 and 2.

**Table 2.** Expansion of Kes 73

Baseline	Observation ID	$\Delta t^a$ (yr)	$\Delta\alpha \cos \delta^b$ (arcsec)	$\Delta\delta^c$	$S^d$	Expansion (%)	Expansion Rate (% yr <sup>-1</sup> )
2000 – 2015	729	14.93	0.038	0.047	$0.966 \pm 0.005$	$0.338 \pm 0.033$	$0.0226 \pm 0.0022$
2006 – 2015	6732	8.91	0.044	0.049	$0.985 \pm 0.006$	$0.204 \pm 0.037$	$0.0229 \pm 0.0042$
(2000+2006) – 2015	729	14.93	0.038	0.046	$0.966 \pm 0.005$	...	...
	6732	8.91	0.043	0.048	$0.985 \pm 0.006$	...	...
	...	...	...	...	...	...	$0.0227 \pm 0.0020$

NOTE— All errors are  $1\sigma$ .

<sup>a</sup>Baseline length.

<sup>b</sup>Alignment error in R.A.

<sup>c</sup>Alignment error in decl.

<sup>d</sup>Model surface brightness scaling.

We first measured expansion independently for the Epoch I - III and Epoch II - III image pairs, with the results listed in the top two rows of Table 2. Alignment errors are  $0''.04$  in R.A. and  $0''.05$  in decl., so the mean alignment error does not exceed  $0''.07$ , significantly less than the mean intrinsic error of  $0''.16$  for *Chandra* pointings (Rots 2009). The surface brightness scaling factor  $S$  is less than unity for both measurements, but only statistical errors are listed in Table 2. Systematic flux calibration errors are significantly larger than statistical errors for  $S$ , most likely at least about 1%, so we find no evidence for temporal variations in either  $S$  or the spatially-integrated flux. Expansion is robustly detected for both image pairs, at  $0.34\% \pm 0.03\%$  for Epochs I and III, and  $0.20\% \pm 0.04\%$  for Epochs II and III. This corresponds to an expansion rate of  $0.023\% \text{ yr}^{-1}$  in both cases.

A joint fit to both Epoch I and Epoch II images, with 7 free parameters (4 image shifts, 2 surface brightness factors  $S$ , and expansion rate) instead of 4 for each image pair, gives the most accurate expansion rate estimate:  $0.0227\% \pm 0.0020\% \text{ yr}^{-1}$ , with other parameters virtually unaffected (Table 2). Since errors listed in Table 2 include only statistical and not systematic errors, the total expansion rate error must be somewhat larger than  $0.002\% \text{ yr}^{-1}$ . One source of systematic errors is the smoothing necessary to obtain the model image shown in Figure 1. This generally biases expansion toward larger values, and this bias increases with the amount of smoothing. The very good agreement found in expansion rates for the Epoch I - III and Epoch II - III image pairs suggests that the magnitude of this bias is much smaller than statistical errors. This source of systematic errors was examined by Borkowski et al. (2016) in their studies of the significantly brighter SNR G11.2–0.3 that expands 20% faster than Kes 73. They found it less important than statistical errors, and this is also expected to hold for Kes 73.

#### 4. BLAST WAVE SPEED AND REMNANT'S AGE

The mean radius of the outer X-ray shell is  $2'$ , so with the measured expansion rate of  $0.023\% \text{ yr}^{-1}$  we arrive at a shell velocity of  $1100 \text{ km s}^{-1}$  at a distance  $d$  of 8.5 kpc (Tian & Leahy 2008). Tian & Leahy (2008) found lower and upper limits to  $d$  to be 7.5 and 9.8 kpc, respectively, so the shell velocity is between  $1000 \text{ km s}^{-1}$  and  $1300 \text{ km s}^{-1}$ . There is faint, clumpy X-ray emission ahead of this shell, so the mean blast wave radius  $r_b$  is larger than  $2'$ , and the blast wave speed must be larger than the mean velocity of the outer shell. Assuming that  $r_b$  is equal to the mean radius of  $2'.5$  for the radio shell (Kumar et al. 2014), we obtain a blast wave speed  $v_b$  of  $1400 \text{ km s}^{-1}$  at 8.5 kpc, or  $1200 - 1600 \text{ km s}^{-1}$  for  $d$  between 7.5 and 9.8 kpc.

The shell expansion rate of  $0.023\% \text{ yr}^{-1}$ , assuming no deceleration, gives an undecelerated remnant's age of 4400 yr. This is essentially the same age (within errors) as the magnetar's spindown age of 4600 yr. This undecelerated age is an upper limit to the remnant's true age  $t_{\text{SNR}}$ , as the blast wave must have been decelerated: the deceleration parameter  $m$  ( $r_b \propto t^m$ ) is less than unity. A conservative lower limit of 1800 yr is obtained by assuming Sedov evolution into a constant-density medium (the standard Sedov model;  $m = 2/5$ ). However, Kes 73 might still be expanding into a circumstellar medium (CSM) produced by mass loss from the progenitor (Chevalier 2005). Assuming Sedov evolution into a steady-state wind ( $m = 2/3$ ), the lower limit to  $t_{\text{SNR}}$  becomes 2900 yr. In principle, the Sedov evolutionary stage, with the ejecta mass negligible compared to the swept-up mass, might not have been attained yet; Kumar et al. (2014) reported the detection of very strong emission from SN ejecta that, if confirmed, would suggest a dynamically young remnant (though see below). The deceleration parameter  $m$  could then be larger than the values of  $2/5$  or  $2/3$  for

the two alternatives just mentioned. Based on our expansion measurements alone, we constrain the age of Kes 73 to be between 2000 and 4000 yr. (We describe further constraints below.) A significantly younger age (even as short as 750 yr) had been previously thought to be viable (Gotthelf & Vasisht 1997; Vink & Kuiper 2006; Tian & Leahy 2008; Kumar et al. 2014), but only the longest of these indirect age estimates are consistent with the measured expansion.

The remnant’s age and evolutionary status can be further constrained with results derived from X-ray spectroscopy. The blast wave speed of  $1400 \text{ km s}^{-1}$  we obtain from our direct expansion measurements is consistent with the values deduced from spectral fits to standard and wind Sedov models by Kumar et al. (2014) of  $v_b$  of  $1200 \pm 300 \text{ km s}^{-1}$  and  $1600 \pm 700 \text{ km s}^{-1}$ , respectively, but the much faster shocks also considered by them are ruled out. For these particular models, Kumar et al. (2014) estimated  $t_{\text{SNR}}$  at  $2100 \pm 500 \text{ yr}$  and  $2600 \pm 600 \text{ yr}$ , again consistent with our results.

The swept-up mass  $M_{sw}$  in Kes 73 is large: Kumar et al. (2014) estimated  $M_{sw}$  at  $(14 - 40) d_{8.5}^{5/2} M_{\odot}$  (where  $d_{8.5}$  is the distance in units of 8.5 kpc) assuming a uniform ambient medium, and several times more than this for the steady-state wind. These mass estimates are based on two-component spectral fits, with one component assumed to represent the SN ejecta, and another the shocked ambient medium. Such spectral decompositions are generally nonunique, and they become even more unreliable when the ejecta mass  $M_{ej} \ll M_{sw}$ . Furthermore, previous work disagrees on the need for elevated abundances; Vink & Kuiper (2006) examined the spatially-integrated spectrum of Kes 73 and found no such need for a two-component model using atomic data from the SPEX package (Kaastra & Mewe 2000), but did require elevated abundances when using an X-ray Sedov model in XSPEC. The latter was based on the XSPEC NEI version 1.1 atomic data also used by Kumar et al. (2014). In order to investigate this issue further, we extracted a spatially-integrated spectrum from the 2015 *Chandra* data, and fit it with an X-ray Sedov model with our improved atomic data. We found no evidence for enhanced abundances, as setting abundances free in spectral fits produced solar or even undersolar abundances depending on the assumed solar abundance set. This resolves the discrepancy between SPEX- and XSPEC-derived abundances found by Vink & Kuiper (2006). We also extracted spectra from several regions investigated by Kumar et al. (2014), and in disagreement with their results we again found no evidence for enhanced abundances in fits using more up-to-date data. Since Kumar et al. (2014) attributed most of the X-ray emission to their SN ejecta component, their swept-up mass estimates (based only on their blast-wave component) must instead be interpreted as lower limits.

The upper limit to  $M_{sw}$  can be estimated from the X-ray emission measure  $EM \equiv \int n_e n_H dV$  ( $n_e$  and  $n_H$  denote electron and hydrogen number densities, respectively) obtained from spectral fits assuming solar abundances. Since there is presumably some ejecta contribution, even if we do

not find obvious overabundances of heavy elements, the mass we obtain from the total emission measure gives an upper limit to the swept-up mass. Vink & Kuiper (2006) obtained  $EM = 2.5 \times 10^{59} d_{8.5}^2 \text{ cm}^{-3}$ , while we find  $3.1 \times 10^{59} d_{8.5}^2 \text{ cm}^{-3}$  from fits to the spatially-integrated *Chandra* spectrum, using an absorbed Sedov model (sedov model in XSPEC), with solar abundances of Grevesse & Sauval (1998) assumed for both the X-ray emitting gas and the (absorbing) ISM. The good agreement between these independent estimates demonstrates that  $EM$  does not depend much on the spectral model. Using  $EM$  for the standard Sedov model and with  $r_b = 2'5 = 6.2 d_{8.5} \text{ pc}$ , we find an upper limit to  $M_{sw}$  of  $69 d_{8.5}^{5/2} M_{\odot}$  (this corresponds to the preshock hydrogen density of  $n_0 = 2.0 d_{8.5}^{-1/2} \text{ cm}^{-3}$ ). For the Sedov wind model, again with  $EM = 3.1 \times 10^{59} d_{8.5}^2 \text{ cm}^{-3}$  and  $r_b = 2'5$ , the upper mass limit becomes  $97 d_{8.5}^{5/2} M_{\odot}$  (using relationships between  $EM$ ,  $r_b$ , and  $M_{sw}$  for the Sedov wind model; e.g., Borkowski et al. 2016), several times larger than found by Kumar et al. (2014) and further strengthening the case for the advanced dynamical age of Kes 73. They also strongly suggest that the blast wave has already entered the ambient ISM; continuing interaction with CSM, possible only for a very massive progenitor, is unlikely because of the very large mass of swept-up CSM required.

We conclude that Kes 73 is in an advanced evolutionary state with  $M_{ej} \ll M_{sw}$  and  $M_{ej} + M_{sw} \lesssim 70 d_{8.5}^{5/2} M_{\odot}$ , and with the blast wave now propagating into ambient ISM with a mean speed of  $v_b = 1400 d_{8.5} \text{ km s}^{-1}$ . With an estimated age of about 2000 yr, it is one of the youngest core-collapse SNRs in our Galaxy.

## 5. DISCUSSION

The mass of the progenitor of Kes 73 and its magnetar is of considerable interest, as most magnetars are thought to result from high-mass progenitors. The high initial spin frequencies attributed to magnetars are expected for progenitors that lost most of their hydrogen envelopes, either through stellar winds or tidal stripping in close binaries, and finally ended their lives as SNe Ib/c. Without extensive envelopes, such stripped-envelope progenitors are less prone to the spin-down experienced by the cores of red supergiant (RSG) progenitors caused by outward transfer of angular momentum to overlying hydrogen envelopes (Heger et al. 2005). Additionally, progenitors of magnetars in binaries can even be spun up through mergers, accretion mass transfer, and tidal synchronization (for a review of scenarios of magnetar formation in binaries, see Popov 2016). Instead of evolving to RSGs, they become compact, hot, and luminous helium stars burning He in their interiors, although perhaps with a residual hydrogen envelope still present in some cases. If sufficiently massive, they are observed as the classical Wolf-Rayet (WR) stars, while more common, low-mass helium stars in binary systems are believed to be the progenitors of most SNe Ib.

If Kes 73 resulted from the explosion of a massive star, it should still be expanding in the progenitor’s stellar wind. The powerful fast winds of very massive stars, both at the main-

sequence (MS) and WR stage, are very effective in blowing large, low-density bubbles in the ambient ISM. A star with an initial mass  $\gtrsim 30M_{\odot}$  may have a strong enough wind to prevent it from becoming a RSG, particularly if it is rapidly rotating as expected for magnetar progenitors. Such a star spends virtually all its life blowing fast stellar winds and inflating its wind-blown bubble to an enormous size. The wind bubble radius  $r_{\text{wb}}$  is  $0.76L_w^{1/5}\rho_0^{-1/5}t_w^{3/5}$ , where  $L_w$  denotes the wind kinetic luminosity,  $\rho_0 = \mu m_p n_0$  is the ambient medium density ( $\mu = 1.4$  denotes the mean mass per hydrogen atom in atomic mass units, and  $m_p$  is the proton mass), and  $t_w$  is time since the onset of the fast wind (Weaver et al. 1977; Chevalier & Liang 1989). For a rotating  $32M_{\odot}$  solar-metallicity Geneva stellar model of Ekström et al. (2012) and Georgy et al. (2012),  $L_w$  is approximately constant and equal to  $10^{36}$  erg s $^{-1}$  during its entire MS lifetime of 6.6 Myr (Georgy et al. 2013). With  $n_0 = 2$  cm $^{-3}$ ,  $r_{\text{wb}}$  becomes 70 pc at the end of the MS stage, and increases further during its post-MS evolutionary stage that ends in a long-lived WR star. The small (6 pc) radius of Kes 73 and the high inferred ambient density  $n_0 = 2$  cm $^{-3}$  are inconsistent with the explosion of a very ( $\gtrsim 30M_{\odot}$ ) massive star. Similar arguments for less massive progenitors, summarized in the Appendix, show that 20 – 30  $M_{\odot}$  stars also should produce wind bubbles inconsistent with observations of Kes 73.

Additional constraints on the SN progenitor can be derived from the lack of clear evidence for elevated abundances. The X-ray spectrum of Kes 73 is dominated by strong lines of Mg, Si, and S, elements that are efficiently produced by massive stars, either through mostly hydrostatic (Mg) or explosive (Si and S) burning. From our Sedov model fits, we can estimate how much Mg, Si, and S (mostly swept-up from the ambient ISM) is present in Kes 73:  $M_{\text{Mg}} = 0.046M_{\odot}$ ,  $M_{\text{Si}} = 0.050M_{\odot}$ , and  $M_{\text{S}} = 0.034M_{\odot}$ . For the nonrotating solar-abundance models of Nomoto et al. (2013) with an explosion kinetic energy of  $10^{51}$  erg, the Mg yields range from 0.03 – 0.12  $M_{\odot}$  for 13 – 20  $M_{\odot}$  models, and become much larger (0.25 – 0.46  $M_{\odot}$ ) for 25 – 40  $M_{\odot}$  models. Similarly, the Si+S yields are 0.10 – 0.15  $M_{\odot}$  for the 13 – 20  $M_{\odot}$  models, and 0.37 – 0.54  $M_{\odot}$  for the 25 – 40  $M_{\odot}$  models. The Si+S yields for stars with lower (13 – 20  $M_{\odot}$ ) masses only marginally exceed  $M_{\text{Si+S}} = 0.084M_{\odot}$  derived by us from the Sedov model fit, but they are much larger for stars with  $M > 20M_{\odot}$ . Only the low (13 $M_{\odot}$  and 15 $M_{\odot}$ ) mass models do not produce more Mg than derived from the observations. If the ejecta mass is sufficiently large ( $\gtrsim 10M_{\odot}$ , as in the single-star models just discussed), there is a possibility that freshly-synthesized Mg, Si, and S might not have been shocked yet, since it can take a long time for the reverse shock to arrive at the remnant’s center and heat the innermost ejecta to X-ray emitting temperatures (Truelove & McKee 1999). But this requires that the Mg-, Si-, and S-rich ejecta have not been significantly mixed outwards, an unlikely prospect given that the magnetar’s relativistic wind efficiently removes heavy elements from the very interior of the SN where they have been produced and mixes them with

the overlying ejecta with the less extreme chemical composition. The lack of clear chemical enrichment is then more consistent with an explosion of a relatively low-mass ( $\lesssim 20M_{\odot}$ ) progenitor than with a more massive ( $\gtrsim 25M_{\odot}$ ) star.

All available evidence points to a relatively low-mass ( $< 20M_{\odot}$ ) progenitor that most likely exploded as a RSG. Long-lived stripped progenitors appear highly unlikely, including those that originated in low-mass stars in binaries (see discussion in Appendix). Stripped progenitors are still possible, but only those that at most underwent only a short-lived post-RSG phase before exploding as a yellow (or blue) supergiant (or potentially even as a more compact He star).

The magnetar’s spindown during or shortly after the SN explosion might have resulted in the injection of a nonnegligible amount of energy into the SN ejecta, thus contributing to the final supernova kinetic energy  $E$ . This energy can now be more reliably estimated assuming Sedov evolution where  $r_b = 12.5E_{51}^{1/5}n_0^{-1/5}t_4^{2/5}$  pc ( $E_{51}$  is  $E$  in units of  $10^{51}$  erg), with  $t_4 \equiv t_{\text{SNR}}/10^4$  yr = 0.18 (from our expansion measurements),  $r_b = 6.2d_{8.5}$  pc, and  $n_0 = 2.0d_{8.5}^{-1/2}$  cm $^{-3}$ . We obtain  $E_{51} \approx 1.9d_{8.5}^{9/2}$ , varying from 1.1 to 3.5 with  $d$  in the 7.5 – 9.8 kpc range.

Based on these explosion energy estimates and the lack of conclusive evidence for ejecta, we conclude that a common (typical) SN IIP could have produced Kes 73, although the contribution of the magnetar to  $E$  is very uncertain as we do not know its initial spin period. The nature of energy deposition of a magnetar into a SN is not clear at this time; if it is primarily electromagnetic, almost all of it could appear as kinetic energy of ejecta (Sukhbold & Thompson 2017). The initial rotational energy  $E_{\text{rot}}$  is  $2 \times 10^{52}P_{\text{ms}}^{-2}$  erg, where  $P_{\text{ms}}$  is the initial spin period in ms. In the extreme case of the magnetar supplying all of  $E$ , we find  $P_{\text{ms}} \gtrsim 3$ , a conservative limit.

Our age determination of about 2000 yr rules out the short end of previously published age ranges for Kes 73. This age is still young enough that it may pose significant problems for theories of magnetar cooling or magnetic-field decay (e.g., Viganò et al. 2013; Beloborodov & Li 2016), given the high magnetic field and quiescent X-ray luminosity of 1E 1841-045.

We conclude that Kes 73 is an undistinguished supernova remnant about 2000 yr old, resulting from an event which is completely consistent with a run-of-the-mill Type IIP explosion of a red supergiant. While Sukhbold & Thompson (2017) suggest that magnetars might power ordinary SN IIP light curves, any RSG phase makes the attainment of ms initial periods highly problematic (Heger et al. 2005). (We note in passing that Heger et al. (2005) find initial rotation periods of progenitors of 20  $M_{\odot}$  or below of 8 – 18 ms, including neutrino effects: possibly too slow for magnetars, but too fast to describe the general pulsar population.) We point out that another magnetar, SGR 1900+14, resulted from a progenitor of only about 17  $M_{\odot}$  (Davies et al. 2009), posing the same problems as 1E 1841-045. Binarity may be necessary to remove the progenitor envelope and allow ms

spin periods (Turolla et al. 2015), though evidence of any surviving companion is scarce. (Clark et al. (2014) report a possible candidate companion for the magnetar CXOU J164710.2–455216.) 1E 1841-045 and SGR 1900+14 may require a separate formation channel.

We acknowledge support by NASA through *Chandra* General Observer Program grant SAO GO5-16070X. The scientific results reported here are based on observations made by the *Chandra* X-ray Observatory. This research has made use of software provided by the *Chandra* X-ray Center (CXC) in the applications packages CIAO and ChIPS. We

acknowledge use of various open-source software packages for Python, including Numpy, Scipy, Matplotlib, Astropy (a community-developed core Python package for Astronomy), and APLpy.<sup>1</sup>

*Software:* CIAO (v 4.8), XSPEC (Arnaud 1996), SPEX (Kaastra & Mewe 2000), Astropy (The Astropy Collaboration 2013), matplotlib (Hunter 2007), Numpy (Walt et al. 2011), Scipy (Jones et al. 2001), APLpy (Robitaille & Bressert 2012)

*Facilities:* CXO

## APPENDIX

Here we describe arguments similar to those in the Discussion above, to show that somewhat lower-mass progenitors than those discussed there ( $\gtrsim 30M_{\odot}$ ) should also produce wind bubbles inconsistent with our observations of Kes 73: an ambient density of  $2 \text{ cm}^{-3}$  and a radius of about 6 pc. For a  $25M_{\odot}$  rotating Geneva model, the brief RSG stage ends long before its explosion because of extensive mass loss, although its wind-blown bubble might be much smaller in size than for the more massive stars. According to Georgy et al. (2013),  $L_w$  is  $\sim 3 - 4 \times 10^{35} \text{ erg s}^{-1}$  during its 7.9 Myr-long MS stage. This is likely an overestimate throughout a significant fraction of its MS evolution when it can be classified as a dwarf (i.e., luminosity class V) and its luminosity  $L$  is less than  $\log L/L_{\odot} \approx 5.2$ , since below this luminosity threshold observations show much weaker than expected winds for OB dwarfs (this is known as the weak wind problem; for a recent review of mass loss in massive stars, see Smith 2014). But this problem is not going to affect the final 15% of the MS stage when its luminosity is above this threshold, and when at the same time it is no longer expected to be a dwarf (Martins & Palacios 2017). Assuming that the wind starts blowing only after the first 6.7 Myr,  $r_{\text{wb}}$  exceeds 20 pc at the end of the MS stage. Further growth of the bubble is expected in its post-MS evolutionary stage, as the star spends  $\sim 50\%$  of its time at this stage blowing a fast stellar wind after evolving to the blue part of the HR diagram following its brief RSG stage. We conclude that single rotating stars that are massive enough to spend at most only a small fraction of their post-MS lifetime as RSGs cannot be progenitors of Kes 73. Since such stars also produce long-lived classical WR stars, the latter are also excluded.

Rotating Geneva models with  $15M_{\odot}$  and  $20M_{\odot}$  spend 1.2 Myr and 0.34 Myr as RSGs, respectively, with the latter's time as an RSG cut short by about one half because of extensive mass loss. With typical stellar motions of  $5 - 10 \text{ km s}^{-1}$  for young stars, the former can travel up to distances equal to Kes 73's diameter. This might be enough for the star with  $15M_{\odot}$  to escape its wind blown bubble, particularly if its size is small because of a very weak stellar wind. With  $L_w$  about  $4 \times 10^{34} \text{ erg s}^{-1}$  on average during its MS lifetime of 13.4 Myr (Georgy et al. 2013), and accounting for the back pressure from the ambient ISM that for relatively weak winds significantly decelerates the bubble's expansion,  $r_{\text{wb}} = 34 \text{ pc}$  according to equation (4.6) in Koo & McKee (1992). Again, this is an overestimate because of the weak wind problem that affects such relatively low-mass stars. A reduction of  $L_w$  by 2 orders of magnitude brings  $r_{\text{wb}}$  down to 7 pc, but even this scale is unrealistically high as even a slow (several  $\text{km s}^{-1}$ ) stellar motion will distort the bubble into an elongated, nonspherical tube-like structure. In order to investigate this problem further, more realistic bubble models are needed, with stellar motions included and allowing for a less extreme reduction in  $L_w$ , but right now we cannot exclude the  $15M_{\odot}$  rotating stellar model as a progenitor for Kes 73 based on the inferred properties of the swept-up ambient ISM.

The  $20M_{\odot}$  rotating star is unlikely to be consistent with the inferred properties of the ambient medium around Kes 73. Because of the weak wind problem,  $L_w$  could possibly be about 2 orders of magnitude less than the value of  $10^{35} \text{ erg s}^{-1}$  obtained with standard mass loss rates (Georgy et al. 2013). But the star is expected to spend at least 15% of its main sequence lifetime of 9.5 Myr as a non-dwarf (Martins & Palacios 2017). Assuming that the wind with  $L_w = 10^{35} \text{ erg s}^{-1}$  starts blowing only after the first 8.1 Myr,  $r_{\text{wb}}$  becomes 18 pc at the end of the MS stage. This is significantly larger than Kes 73's radius, although  $r_{\text{wb}}$  might have been overestimated if the weak-wind problem persists beyond dwarfs to higher luminosity classes (Smith et al. 2017). After the RSG stage, the star spends  $2 \times 10^5 \text{ yr}$  blowing a fast wind with an average mass-loss rate  $\dot{M}$  of  $5 \times 10^{-6} M_{\odot} \text{ yr}^{-1}$ , eventually becoming a short-lived WR star. Assuming  $v_w = 1000 \text{ km s}^{-1}$ ,  $L_w$  exceeds  $10^{36} \text{ erg s}^{-1}$ . Such a strong wind is capable of blowing a bubble slightly larger than the remnant's size even if the RSG were able to escape the larger bubble created at the end of the MS stage. But even if a wind-blown bubble were just a few pc in radius because of a slightly weaker than assumed wind, a remnant with a particularly prominent limb-brightened shell is expected after the SN explosion, as observed in G11.2–0.3 (this CC SNR was inferred to originate from an explosion within a small bubble; Borkowski et al. 2016). The shell of Kes 73 is not

<sup>1</sup> APLpy is an open-source plotting package for Python hosted at <http://aplpy.github.com>.

as prominent as in G11.2–0.3, but further work is needed to investigate whether an explosion in a small bubble blown shortly before the SN explosion is inconsistent with the remnant’s X-ray and radio morphologies.

Less powerful winds of low-mass He stars in binaries blow smaller bubbles than the classical WR stars, but their radii are still substantial. For a representative low-mass SN Ib progenitor model with solar abundances, a main-sequence mass of  $12M_{\odot}$ , and a He core mass  $\sim 4M_{\odot}$ , Götberg et al. (2017) estimated  $\dot{M}$  at  $2.5 \times 10^{-7} M_{\odot} \text{ yr}^{-1}$  during the core He-burning stage. All luminous helium stars lose mass in fast ( $v_w \sim 1000 \text{ km s}^{-1}$ ) stellar winds. Assuming  $v_w = 1000 \text{ km s}^{-1}$ ,  $L_w = 8 \times 10^{34} \text{ erg s}^{-1}$ , and again with  $n_0 = 2 \text{ cm}^{-3}$ ,  $r_{\text{wb}} = 14t_{w,\text{Myr}}^{3/5} \text{ pc}$ , where  $t_{w,\text{Myr}}$  is  $t_w$  in Myr. The long (1.5 Myr) duration of the He-burning stage means that a large ( $r_{\text{wb}} \gtrsim 10 \text{ pc}$ ) bubble is expected. The small (6 pc) radius of Kes 73 and the high inferred ambient density  $n_0 = 2 \text{ cm}^{-3}$  appear inconsistent with an explosion within a bubble blown by a long-lived low-mass He star progenitor. Still, there are considerable gaps in our knowledge of these relatively low-luminosity stars (e.g., Yoon 2015), so this conclusion is not as robust as for the single massive stars that end their lives as long-lived WR stars.

## REFERENCES

- Arnaud, K. A. 1996, in ASP Conf. Ser. 101, *Astronomical Data Analysis and Systems V*, ed. G. Jacoby & J. Barnes (San Francisco, CA: ASP), 17
- The Astropy Collaboration, Robitaille, T. P., Tollerud, E. J., et al. 2013, *A&A*, 558, 33
- Badenes, C., Borkowski, K. J., Hughes, J. P., et al. 2006, *ApJ*, 645, 1373
- Beloborodov, A. M., & Li, X. 2016, *ApJ*, 833, 261
- Borkowski, K. J., Reynolds, S. P., Hwang, U., et al. 2013, *ApJL*, 771, L9
- Borkowski, K. J., Reynolds, S. P., & Roberts, M. S. E. 2016, *ApJ*, 819, 160
- Carlton, A. K., Borkowski, K. J., Reynolds, S. P., et al. 2011, *ApJL*, 737, L22
- Cash, W. 1979, *ApJ*, 228, 939
- Chevalier, R. A. 2005, *ApJ*, 619, 839
- Chevalier, R. A., & Liang, E. P. 1989, *ApJ*, 344, 332
- Clark, J. S., Ritchie, B. W., Najarro, F., Langer, N., & Negueruela, I. 2014, *A&A*, 565, 90
- Davies, B., Figer, D. F., Kudritzki, R. P., et al. 2009, *ApJ*, 707, 844
- Duncan, R. C., & Thompson, C. 1992, *ApJL*, 392, L9
- Ekström, S., Georgy, C., Eggenberger, P., et al. 2012, *A&A*, 537, 146
- Ferrario, L., & Wickramasinghe, D. 2006, *MNRAS*, 367, 1323
- Georgy, C., Ekström, S., Meynet, G., et al. 2012, *A&A*, 542, 29
- Georgy, C., Walder, R., Folini, D., et al. 2013, *A&A*, 559, 69
- Götberg, Y., de Mink, S. E., & Groh, J. H. 2017, submitted to *A&A* (arXiv:1701.07439)
- Gotthelf, E. V., & Vasisht, G. 1997, *ApJL*, 486, L133
- Grevesse, N., & Sauval, A. J. 1998, *SSRv*, 85, 161
- Gullón, M., Pons, J. A., Miralles, J. A., et al. 2015, *MNRAS*, 454, 615
- Heger, A., Woosley, S. E., & Spruit, H. C. 2005, *ApJ*, 626, 350
- Hunter, J. D. 2007, *Comp. Sci. Engr.*, 9.3, 90
- Jones, E., Oliphant, T., Peterson, P., et al. 2001, <http://www.scipy.org>
- Kaastra, J. S., & Mewe, R. 2000, in *Atomic Data Needs for X-ray Astronomy*, ed. M. A. Bautista, T. R. Kallman, & A. K. Pradhan (Washington, DC: NASA), 161
- Kaspi, V. M., & Beloborodov, A. M. 2017, *ARA&A*, 55, in press
- Koo, B.-C., & McKee, C. F. 1992, *ApJ*, 388, 93
- Krishnamurthy, K., Raginsky, M., & Willett, R. 2010, *SIAM J. Imaging Sci.*, 3, 619
- Kumar, H. S., Safi-Harb, S., Slane, P. O., & Gotthelf, E. V. 2014, *ApJ*, 781, 41
- Li, J., Rea, N., Torres, D. F., & de Oña-Wilhelmi, E. 2017, *ApJ*, 835, 30
- Martin, J., Rea, N., Torres, D. F., & Papitto, A. 2014, *MNRAS*, 444, 2910
- Martins, F., & Palacios, A. 2017, *A&A*, 598, 56
- Nomoto, K., Kobayashi, C., & Tominaga, N. 2013, *ARA&A*, 51, 457
- Olausen, S. A., & Kaspi, V. M. 2014, *ApJS*, 212, 6
- Popov, S. B. 2016, *AApTr*, 29, 183
- Robitaille, T., & Bressert, E. 2012, *Astrophys. Source Code Lib.*, record ascl:1208.017
- Rots, A. 2009, *Determining the Astrometric Error in CSC Source Positions*, [cxc.harvard.edu/csc/memos/files/Rots\\_CSCAstrometricError.pdf](http://cxc.harvard.edu/csc/memos/files/Rots_CSCAstrometricError.pdf)
- Smith, N. 2014, *ARA&A*, 52, 487
- Smith, N., Groh, J. H., France, K., & McCray, R. 2017, *MNRAS*, 468, 2333
- Smith, R. K., Brickhouse, N. S., Liedahl, D. A., & Raymond, J. C. 2001, *ApJL*, 556, L91
- Spruit, H.C. 2008, in *40 Years of Pulsars: Millisecond Pulsars, Magnetars and More*, eds. C. Bassa, Z. Wang, A. Cumming, & V.M. Kaspi (American Institute of Physics Conf. Ser.), 983, 391
- Spruit, H. C. 2009, in *Proc. IAU Symp. 259, Cosmic Magnetic Fields: From Planets, to Stars and Galaxies*, ed. K. G. Strassmeier, A. G. Kosovichev, & J. E. Beckman (Cambridge: Cambridge University Press), 61
- Sukhbold, T., & Thompson, T. A. 2017, submitted to *MNRAS* (arXiv:1704.06682)



- Tian, W. W., & Leahy, D. A. 2008, *ApJ*, 677, 292
- Truelove, J. K., & McKee, C. F. 1999, *ApJS*, 120, 299
- Turolla, R., Zane, S., & Watts, A. L. 2015, *RPPh*, 78, 116901
- Viganò, D., Rea, N., Pons, J. A., et al. 2013, *MNRAS*, 434, 123
- Vink, J., & Kuiper, L. 2006, *MNRAS*, 370, L14
- Walt, S. v. d., Colbert, S. C., & Varoquaux, G. 2011, *Comp. Sci. Eng.* 13.2, 22
- Weaver, R., McCray, R., Castor, J., Shapiro, P. R., & Moore, R. T. 1977, *ApJ*, 218, 377
- Williams, B. J., Borkowski, K. J., Ghavamian, P., et al. 2013, *ApJ*, 770, 129
- Yeung, P. K. H., Kong, A. K. H., Tam, P. H. T., et al. 2017, *ApJ*, 837, 69
- Yoon, S.-C. 2015, *PASA*, 32, e015
- Younes, G., Kouveliotou, C., & Kaspi, V. M. 2015, *ApJ*, 809, 165